

Structure-stiffness relation of live mouse brain tissue determined by depth-controlled indentation mapping

Nelda Antonovaite^{1,*}, Steven V. Beekmans¹, Elly M. Hol^{2,3,4}, Wytse J. Wadman⁴, and Davide Iannuzzi¹

¹Department of Physics and Astronomy and LaserLab Amsterdam, Vrije Universiteit Amsterdam, De Boelelaan 1085, 1081 HV, Amsterdam, Netherlands, nelda.antonovaite@student.vu.nl

²Department of Translational Neuroscience, Brain Center Rudolf Magnus, University Medical Center Utrecht, 3584 CG Utrecht, The Netherlands

³Netherlands Institute for Neuroscience, An Institute of the Royal Netherlands Academy of Arts and Sciences, 1105 BA Amsterdam, The Netherlands

⁴Center for Neuroscience, Swammerdam Institute for Life Sciences, University of Amsterdam, 1098 XH Amsterdam, The Netherlands

February 8, 2018

Abstract

The mechanical properties of brain tissue play a pivotal role in neurodevelopment and neurological disorders. Yet, at present, there is no consensus on how the different structural parts of the tissue contribute to its stiffness variations. Here, we have gathered depth-controlled indentation viscoelasticity maps of the hippocampus of isolated horizontal live mouse brain sections. Our results confirm the highly viscoelastic nature of the material and clearly show that the mechanical properties correlate with the different morphological layers of the samples investigated. Interestingly, the relative cell nuclei area seems to negatively correlate with the stiffness observed.

Brain tissue consists of neuronal cell bodies, their processes (dendrites and axons, myelinated or not, which form either sparse branches and arborizations or dense fiber bundles), the interconnecting extracellular brain matrix (ECM), glial cells, blood vessels, and extracellular fluid. Each of these components may have a different influence on the local mechanical properties of the tissue, which, in turn, regulate a wide variety of very relevant mechanotransduction phenomena. For instance, mechanical signals are known to play a role in multiple vital processes of neural cells [1, 2], whereas neuronal growth, neurite extension, arborization patterns, neuronal traction forces, and the stiffness of individual neurons and glial cells were all found susceptible to the stiffness of the substrate [3–11]. Furthermore, an abnormal mechanical environment (emerging as a result of internal or external forces, changes in the composition of the ECM, or changes in osmotic conditions) can disrupt normal brain function and neurodevelopment, and can alter progression of neurological disorders [12–14]. It is therefore commonly agreed that a deep knowledge of the correlation between brain composition and mechanical properties of the tissue would enable neuroscientists to shed light on how mechanotransduction phenomena contribute to the functioning of the brain. Furthermore, a quantitative assessment of the viscoelasticity characteristics of the different regions of the brain could pave the way for the improvement of computational brain injury models [15], the engineering of brain

phantoms for surgical practise [16, 17], the design of mechanically matched brain implants [18], and the production of soft substrates that could mimic different mechanical environments for investigations of stiffness-dependent neural stem cell differentiation [19–21] and neuronal and glial cell morphology [22]. Yet, at present, the relation between mechanical properties and cytoarchitecture is still largely unknown.

Previous studies on brain mechanics have been mainly limited to the comparison between white and gray matter, with results that are either inconsistent or lack quantitative structure analysis [23–31]. Only recently, one study has shown that the mechanical properties correlate with myelin content in bovine brain [24], while stiffness was found to scale with the cell nucleus area in spinal cord of mouse and retinal ruminant tissue [30, 32]. Even though differences in mechanical properties of large hippocampal regions such as cornu ammonis (CA) fields and the dentate gyrus (DG) have been reported previously [33–37], this set of data is not sufficient to completely determine the correlation between the morphological structure of the brain and its mechanical properties.

From a purely technical perspective, this literature gap is not surprising. Brain tissue is a highly viscoelastic, non-linear, anisotropic material [27, 38–42], and, because of its cellular heterogeneity, low stiffness, and rapid degradation, it is one of the most difficult (bio)materials to mechanically test. Macroscopic tests (such as shear rheology, compression testing, and tension testing) can only measure the mechanical properties of large samples, and, for this reason, cannot provide information on the local features of the tissue. Atomic force microscope (AFM) indentation, on the contrary, makes use of a small radius tip to locally probe the mechanical response of a material to a compressive stress, and, therefore, seems to be more suitable to assess how the mechanical properties of the different regions of the brain may be influenced by the underlying morphological composition [43]. Unfortunately, the results reported in the literature do not always agree with each other, as witnessed by the wide range of stiffness values reported [39, 42, 44].

Tantalized by this challenge, we have explored whether a recently introduced mechanical testing technique, known as ferrule-top dynamic indentation [45, 46], could provide a better insight on the correlation between the composition of brain tissue and its viscoelastic properties. The technique used in our experiment is quite similar to AFM indentation. However, with respect to the latter, it offers one key advantages, in that the position of the cantilever is monitored by means of optical fiber interferometry rather than the optical triangulation technique used in AFM. As already showed in several papers [45–48], this method is suited for the implementation of highly stable electromechanical feedback loops, which, in turn, guarantee better measurement protocols, including dynamic mechanical analysis at controlled indentation depth.

In this paper, we demonstrate that, using our deep, depth-controlled indentation method, one can obtain high spatial resolution viscoelasticity map of a mouse hippocampus slice. The map clearly emphasizes how the different structural layers give rise to different mechanical properties. Our results further show that brain tissue appears stiffer as the indentation depth or frequency increase – a result that confirms the non-linear viscoelastic nature of the brain tissue. Finally, calculating the mean measured stiffness of eleven anatomical subregions, and comparing it with the estimated nuclear densities, we can infer that densely packed cell layers may actually have lower stiffness than more disperse ones – a result that seems to contradict the commonly accepted assumption that brain tissue stiffness is dominated by cell bodies [3, 30].

Results

Mechanical heterogeneity of hippocampus agrees with anatomical region boundaries

Viscoelasticity maps of live brain sections were obtained by means of ferrule-top depth-controlled indentation [45, 46]. The image of one of the samples used in the experiment, along with a typical $50\ \mu\text{m} \times 50\ \mu\text{m}$ grid of indentation locations, can be seen in Fig. 1a. We refer the reader to the method section for further details on instrumentation and protocol.

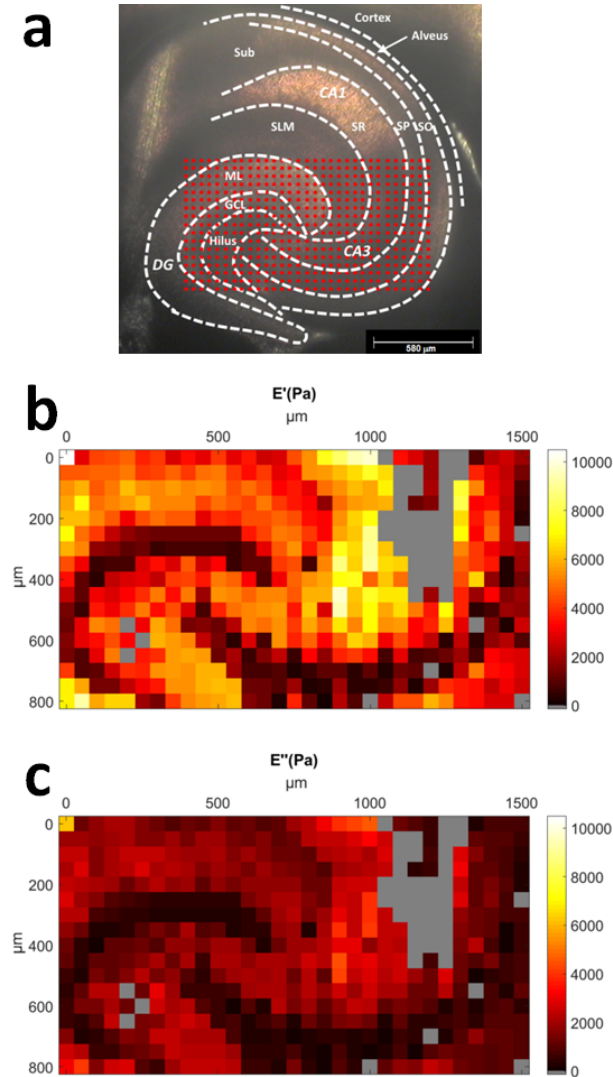


Figure 1: (a) Microscope image of one of the slices used in this experiment, along with a typical $50\ \mu\text{m} \times 50\ \mu\text{m}$ indentation grid (red dots). Dashed lines indicate boundaries of morphologically distinct anatomical regions. Abbreviations: Sub - subiculum, SLM - stratum lacunosum moleculare (SLM), SR - stratum radiatum, SP - stratum pyramidale, SO - stratum oriens, ML - molecular layer, GCL - granule cell layer; large regions: DG - dentate gyrus, CA - cornus ammonis. (b, c) Color-coded map of storage E' (b) and loss modulus E'' (c) in Pa over the DG and CA3 field of the hippocampal formation obtained with oscillatory ramp depth-controlled indentation strokes (see Online Methods) with $0.2\ \mu\text{m}$ oscillation amplitude, $5.62\ \text{Hz}$ oscillation frequency, and 9% strain. Gray color indicates failed measurements.

Fig. 1b and c show the viscoelasticity maps (E' = storage modulus; E'' = loss modulus) over the DG and the proximal portion of CA3 field of the hippocampus obtained from a

horizontal mouse (9 months old) brain slice around 3 to 4 mm in the dorsal-ventral position. The representative maps were obtained with depth-controlled oscillatory ramp indentation strokes (see Online Methods) at an estimated strain of 9%. Similar maps, albeit focused on smaller areas, were obtained in 8 other slices (7 slices from 6 months old mice and 1 slice from 9 months old mice) out of 11 tested. As for the remaining 2 (both obtained from 9 months old mice), the data looked rather scrambled and not reproducible, probably because the sample was not perfectly adhering on the substrate.

In Fig. 1, one can clearly identify multiple areas with distinctive mechanical features. The shape of these regions agrees well with the morphological heterogeneity of anatomical subregions (see Fig. 1a), including the U-shaped structure of the molecular layer (ML) and of the granule cell layer (GCL) enclosing the hilus, and the laminar organization of strata (layers): oriens (SO), pyramidale (SP), radiatum (SR) and lacunosum-moleculare (SLM).

Brain tissue is non-linear viscoelastic

To confirm that ferrule-top depth-controlled dynamic indentation is capable of capturing the non-linear viscoelastic nature of the brain tissue, we analyzed all the data obtained from the hippocampus together (i.e., without subdivision into layers). The averaged storage and loss moduli over frequency (obtained with the frequency sweep method) and strain (obtained with the oscillatory ramp method) are shown in Fig. 2. The frequency sweep data reveal a stiffening of the tissue with increasing indentation frequency, whereas the depth profiles from the oscillatory ramp testing show a stiffening with strain.

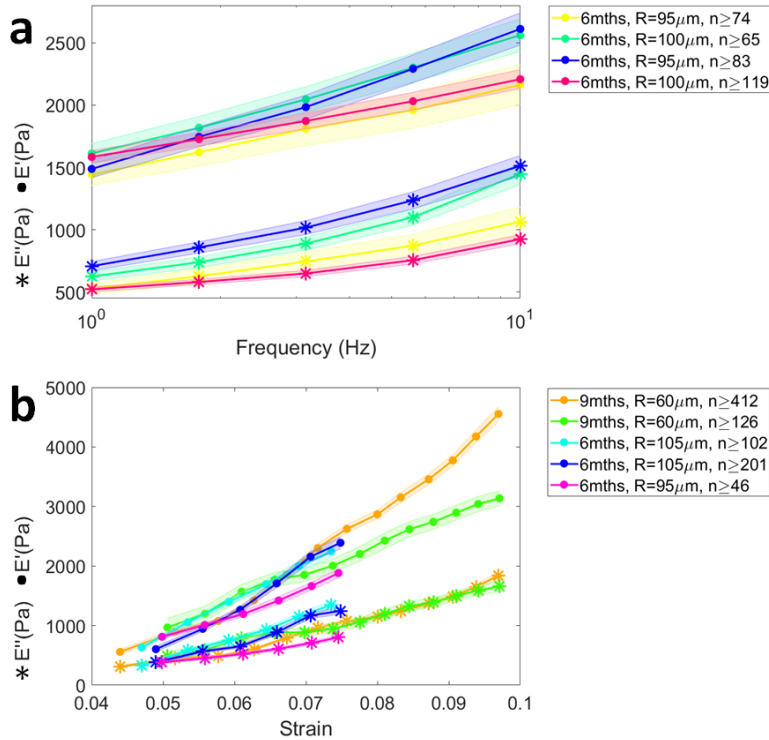


Figure 2: Non-linear viscoelastic properties of hippocampus obtained with dynamic indentation-controlled testing: frequency sweep (a) and oscillatory ramp (b). (a) Storage and loss moduli E' and E'' increase over a frequency range of 1-10 Hz (data averaged over hippocampus; measured at $\sim 7\%$ strain, 0.2 μ m oscillation amplitude; note the logarithmic scale on the x-axis). (b) E' and E'' increase over the strain range of 4-10% (measured at 5.62 Hz oscillation frequency, 0.2 μ m oscillation amplitude). The age of the animals is specified in the legend. Shaded zones indicate the standard error of the mean, whereas R indicates the radius of the indenting tip and n the number of measurement points.

Regional viscoelastic properties are reproducible

To test inter-animal variability of the mechanical properties measured in different brain areas, we developed a protocol to identify anatomical regions and indentation locations. The coordinates of the XYZ micromanipulator were calibrated, prior to the measurements, using the image of the tip of the probe in the camera of the inverted microscope. At the end of the indentation measurement, each measured brain section was formalin-fixed and stained for nuclei and neurofilaments, which indicates the neuronal axons (see Fig. 3, Online Methods). Differences in cell densities and organization of axons, visualized in fluorescent images, allowed us to draw boundaries between anatomical regions and overlay them with the image of the slice from the inverted microscope. Next, each indentation location was assigned to the corresponding anatomical region and the viscoelastic properties were averaged over these regions. The layered composition of the cortex areas varied between slices and were treated as a single region.

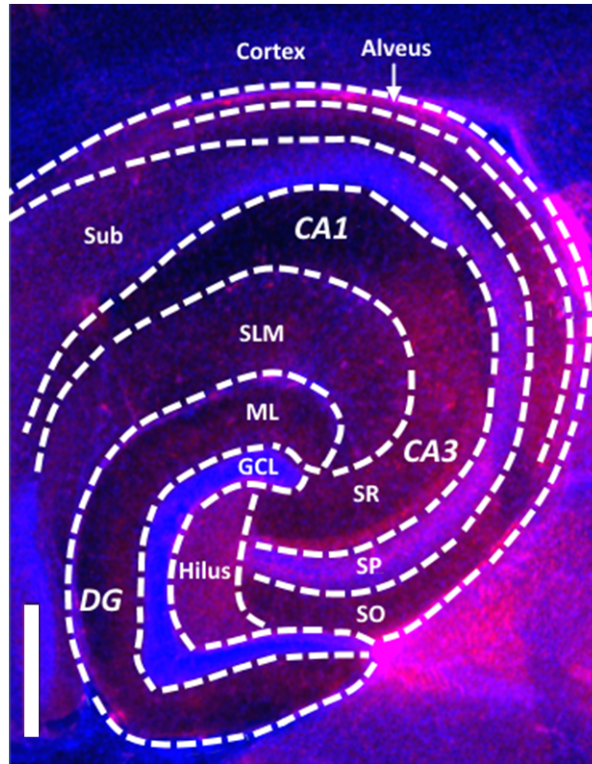


Figure 3: Fluorescent microscopy image of the hippocampus, visualizing cell nuclei (blue) and neurofilaments (red). Dashed lines indicate boundaries of morphologically distinct anatomical regions. Scale bar = 200 μm .

Fig. 4 shows the value of E' at 7.3% strain and 5.62 Hz frequency, averaged over all the slices, for each of the different regions identified with the staining procedure, plotted from the softest to the stiffest in increasing stiffness order (as determined by the results obtained with the oscillatory ramp method). As expected from the viscoelasticity maps, the mechanical properties of the brain tissue appear highly heterogeneous. Both measuring methods (oscillatory ramp and frequency sweep) highlight the same trend in the mechanical properties of the different regions investigated, with the exception of the SLM region, where the frequency sweep method seems to indicate a decrease in stiffness that the oscillatory ramp does not detect.

To compare the local storage modulus measured in different slices, we performed one-way ANOVA followed by *post hoc* test for each region (Online Methods). The results are indicated on top of Fig. 4 as a ratio between the number of significantly different pairs over the total number of pairs used for the comparison. Remarkably, only 17% of the tested pairs were significantly different, especially if one considers that 57% of these variations stems from the comparison of

data obtained with different experimental methods (frequency sweep versus oscillatory ramp). This result confirms that, in our experiments, there is a good inter-animal reproducibility of the results.

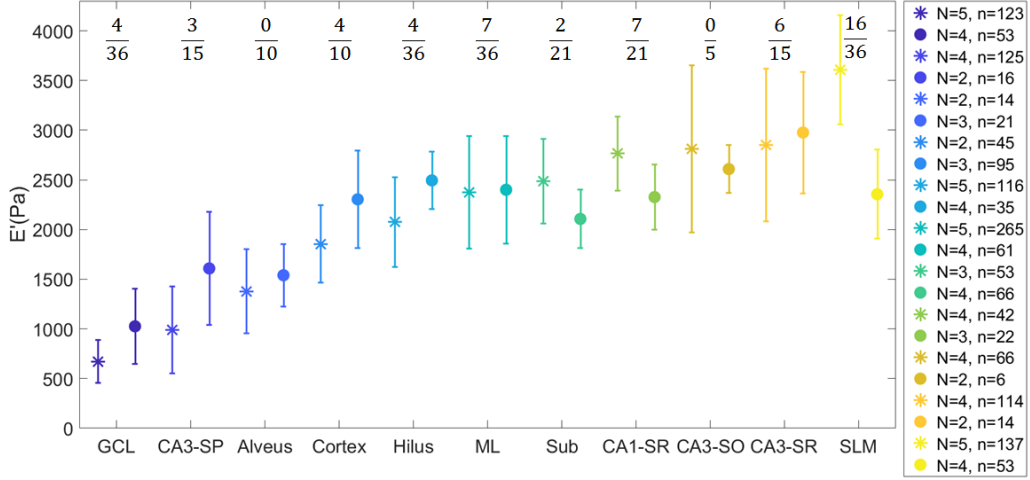


Figure 4: Comparison of the weighted means of the storage modulus of different brain regions obtained with an oscillatory ramp (stars) or a frequency sweep (dots) approach at 7.3% strain and 5.62 Hz frequency. The legend indicates the number of slices N used to calculate the weighted mean and the total number of measurement points n . The fraction on top indicates the number of significantly different pairs over the total number of pairs analyzed with *post hoc* test. Error bars are SE of the weighted mean.

Relative area of nuclei negatively correlates with mechanical properties

The relation between stiffness and underlying morphological structure was assessed by evaluating the percentage of area covered by cell nuclei of each of the regions investigated. A horizontal Nissl-stained slice from a similar location within the brain was used to obtain relative nuclei area A_{rel} in each measured region (see Online Methods). Afterwards, the weighted mean of the storage modulus of all slices was plotted against A_{rel} (Fig. 5). In this graph, one can identify three groups. The first group from the left, which includes the SR of the CA1 and the CA3 fields, the SO-CA3 and the SLM, appears to be the stiffest (~ 2614 - 3260 Pa) and relatively cell-free ($A_{rel} = 2.6$ - 4.9%). The second group, which includes the cortex, the hilus and the subiculum has intermediate stiffness (~ 2159 - 2276 Pa) and intermediate A_{rel} (20.7 - 31.8%). Finally, the GCL, which has the highest A_{rel} (95.1%), also appears to have the softest mechanical properties (~ 779 Pa), followed by the SP-CA3 with an A_{rel} of 82.8% (~ 1059 Pa). While the SP-CA3 layer has a high density of both axons and cells, we could not evaluate the contribution of axons to the stiffness. However, alveus, containing mostly fibers and low A_{rel} (9.4%) appears to be softer (~ 1475 Pa) than all other high-intermediate stiffness and low-intermediate A_{rel} regions.

Remarkably, by carrying out a linear regression on all data of Fig. 5, one can show that there is a strong negative correlation between the stiffness of a brain region and its relative area of nuclei (Pearson's correlation coefficient $r = -0.85$), which is even stronger if the Alveus is excluded from the analysis ($r = -0.97$).

For future reference, in Fig. 6, we provide a map of the storage modulus of the different brain tissue regions as reconstructed with the values reported in Fig. 5.

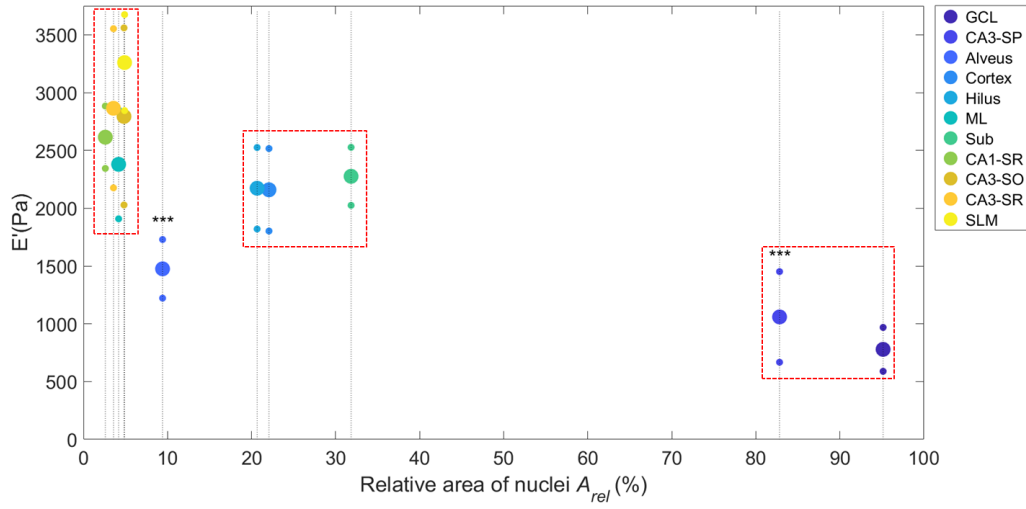


Figure 5: Weighted means of the storage modulus (combined data from all slices) plotted as a function of relative area of nuclei. Stars indicate regions with high axon density. Red dashed squares mark three groups based on stiffness and A_{rel} (from left to right): stiff and low- A_{rel} , intermediate stiffness- A_{rel} , soft and high- A_{rel} . Error bars are SE of the weighted mean.

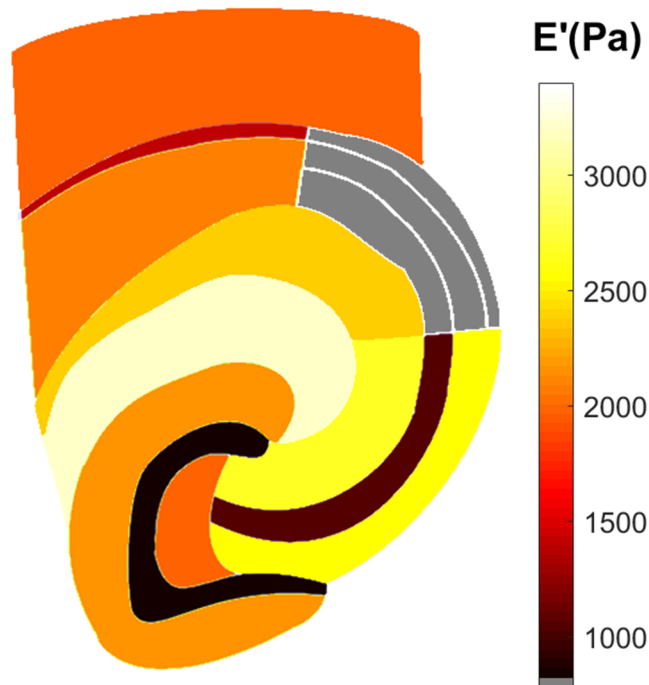


Figure 6: Reconstructed storage modulus map of brain tissue regions based on a weighted mean of 9 slices. Gray color indicates regions that were not measured.

Discussion

In this study, we have used a ferrule-top indentation approach to gather viscoelastic maps of mouse brain tissue in their physiological state. The size of the indentation sphere and the depth of indentation were selected to ensure that the measurements could provide the tissue mechanical features of the subregional area of the tested sample. High spatial resolution (50 μm) of indentation mapping allowed us to find a clear correlation between indented regions and viscoelastic properties. The same relationship was reproduced on multiple slices by means of different testing method (frequency sweep and oscillatory ramp).

Our measurements show that both storage and loss moduli increase with strain. We can thus confirm that brain tissue is a non-linear material, as already reported in other studies [30,34,36]. Furthermore, performing the first localized frequency-domain indentation measurements on brain slices ever reported in the literature, we could observe that, in the 1-10 Hz range, both storage and loss moduli increase with indentation frequency – a viscoelastic behavior that was previously observed as a stress relaxation, creep response and change in strain-rate sensitivity in other indentation experiments [23, 25, 34, 35, 49]. In quantitative terms, it is interesting to note that, converting the averaged values of E' obtained in our measurements (Fig. 2a) to shear moduli G' by dividing E' by $2(1+\nu)$ (where $\nu = 0.5$ is the Poisson's ratio of compressibility), one obtains values for G' of $0.5\text{-}0.8\pm 0.1$ kPa, which is in good agreement with macroscopic (i.e., not localized) frequency sweep measurements reported in the literature [28, 31, 50–56]. A direct comparison with other local measurements is unfortunately not possible, because the latter have been either performed on different kind of samples (different age, species, slicing direction) or under very diverse indentation stroke protocols, which, because of the highly viscoelastic behavior of the material, give rise to very different results [23–26, 29, 33–36, 57].

Our viscoelasticity maps further reveal that the stiffness of the hippocampal subregions and the cortex negatively correlates with the relative area of nuclei; in other words, higher cell body density corresponds to a softer tissue. This is consistent with the study on single cortical neurons where soma has been found to be significantly softer than neurites [58]. However, our findings are in contrast with previous studies, which found a positive correlation between stiffness and cell nucleus area on the spinal cord of the adult mouse, retina of the ruminant and embryonic brain of *Xenopus* [3,30,32]. Furthermore, granular cell layer in coronal hippocampal slices of the juvenile rats was also shown to be stiffer than hilus [21]. While different CNS tissue composition might be the reason for the discrepancy between our results and those reported in the literature, it is worth stressing that our indentation protocol significantly differs with respect to that used in previous studies. The AFM system used in previous studies relies on small beads (radius < 20 μm) and on a stroke that moves the probe at a constant speed of 10 $\mu\text{m/s}$ until a predefined maximum force is reached (with the maximum force being on the order of several nN). We estimate that the contact radius must then be smaller than 10 μm , with an indentation depth of less than 4 μm . It is thus legitimate to ask whether this kind of AFM measurements probe the tissue properties or, actually, only indent the first layer of cells that lie on the surface. Furthermore, the piezo-control testing used in AFM measurements results in different strain rates and indentation depth for different values of stiffness of the tissue indented; under the same stroke protocol, a softer tissue will experience a higher strain rate and a larger indentation depth. In contrast, our deep, indentation-control testing protocol assures constant indentation depth and constant indentation speed. Furthermore, with indentation beads in the range of 60-105 μm , strain of $\sim 7\%$, and indentation depth between 8-11 μm (which results in a contact radius between 20 and 40 μm), we are sure to measure at the scale of the tissue. Therefore, we suggest that the opposite relationship between stiffness and areas of cell nuclei observed in our experiment might be at least partially due to the difference in the scale probed and/or in the very same testing method.

Our data is not sufficient to fully explain why low nuclear density regions translate into stiffer tissues. At first, one may think that the increase of stiffness with the decrease of nuclear density be due to the role of the perineural nets (PNNs). However, it has been showed that this component lacks fibrous proteins [59], and, therefore, should not support mechanical loading. Another component that may play a role in the mechanical properties of the brain tissue is myelin, as it has been shown that brain stiffness increases with myelin content [24, 36]. Yet, our results indicate that the bundle of myelinated fibers in the alveus and the tract of mossy fibers along the SP in the CA3 field are actually softer. One may thus speculate whether the mechanical properties of the brain tissue as observed in our experiment are rather due to the fact that regions with low nuclear density host a larger amount of sparsely distributed axons and dendrites under tension [60–66], which may in turn give rise to a stiffer material. To confirm or reject this hypothesis, it is imperative to perform new measurements that could directly correlate stiffness with axon density and orientation.

Methods

Sample preparation

C57Bl/6 mice were sacrificed at an age of 6 or 9 months. All experiments were performed in accordance with protocols and guidelines approved by the Institutional Animal Care and Use Committee (UvA-DEC) operating under standards set by EU Directive 2010/63/EU. All efforts were made to minimize the suffering and number of animals. The mice were decapitated, the brain was removed from the skull and stored in ice-cold ACSF containing (in mM): 120 NaCl, 3.5 KCl, 5 MgSO₄, 1.25 NaH₂PO₄, 2.5 CaCl₂, 25 NaHCO₃, and 10 glucose oxygenated with 95% O₂/5% CO₂ (~310 mOsmol/kg and ~pH 7.4). Slices were cut in a horizontal plane with a thickness of approximately 300 μ m using a VT1200S vibratome (Leica Biosystems, Nussloch, Germany). Afterwards, a single brain tissue slice was placed in a perfusion chamber maintained at ~20 °C and supplied with carbogen saturated ACSF solution at 1 ml/min flow rate (gear pump MCP-Z standard, Ismatec). The glass bottom of the chamber was coated with 0.05% polyethylenimine for the adhesion with the sample, which was also pressed down from the top with a 2 mm spaced harp to ensure the stability. After acclimatization for 1 h, indentation measurements were performed within 8 h.

Imaging and immunofluorescence

An inverted microscope (Nikon TMD-Diaphot, Nikon Corporation, Japan) was used to image the slice during the measurements with a 2 \times magnification objective (Nikon Plan 2X, Nikon Corporation, Japan). Images were recorded with a CCD camera (WAT-202B, Watec). After the measurements, slices were fixed in 4% PFA overnight at 4 °C. The sections were washed 3 \times 10 min in PBS solution (0.01 M, pH = 7.4) and subsequently blocked for 2 h with 10% normal donkey serum (NDS), 0.25% Triton in PBS solution. After, slices were incubated overnight at 4 °C with primary antibody against neurofilament 160 kDa (NN18 N5264, Sigma Aldrich, 1:1000 dilution), 3% NDS and 0.25% Triton in PBS solution. Consequently, slices were washed 3 \times 10 min in PBS solution and incubated for 2 h in PBS solution with DNA stain (Hoechst 33342, Invitrogen, dilution 1:2000), the secondary antibody Cy3-conjugated donkey anti-mouse IgG (Jackson Immuno Research, 1:1400 dilution), 1% NDS and 0.025% Triton. Finally, sections were washed 3 \times 10 min in PBS and mounted with a glass coverslip in Vectashield (Vector Laboratories). Fluorescent images were obtained with Leica DMRE fluorescence microscope (Leica Microsystems, Wetzlar, Germany) and overlaid with the previously obtained bright-field images to identify anatomical regions of measured locations. Immunofluorescently-labeled slices

were too thick for objective calculation of cell density and, thus, percentage of area covered by nuclei was estimated for each region from a Nissl stained image of horizontal 25 μm thickness adult-mouse brain section (<http://brainmaps.org>, [67]):

$$A_{rel} = \frac{A_{nuclei}}{A_{total}}, \quad (1)$$

where A_{nuclei} is the area covered by nuclei in the region and A_{total} is the total area of that region (processed with image J).

Dynamic indentation setup and measurement protocol

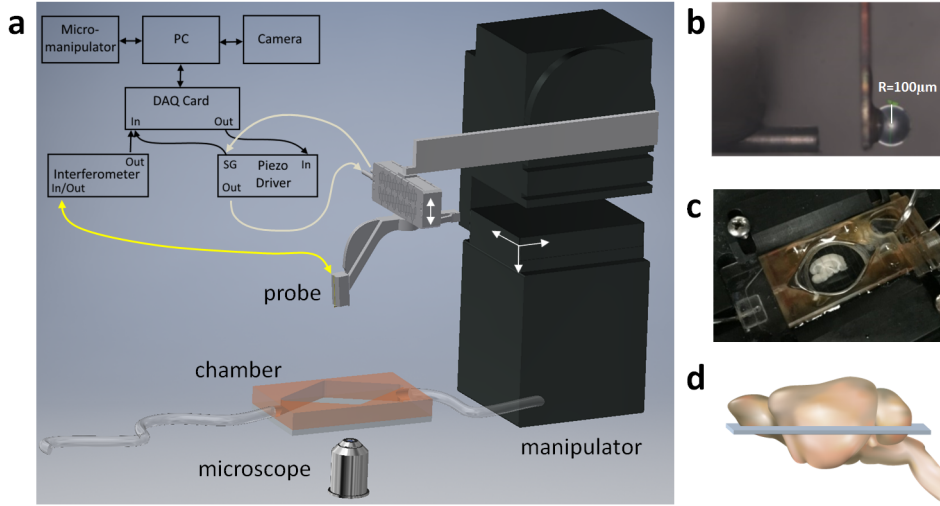


Figure 7: Schematic view of the dynamic indentation mapping setup. A ferrule-top probe (a) is equipped with an optical fiber for interferometric readout of the cantilever position and with a spherical tip to indent the sample (b). The probe is mounted on a piezoelectric transducer (a) for controlled movement during an indentation measurement. A brain slice is submerged in the perfusion chamber and fixed with the harp (c). The slice is imaged with an inverted microscope (a) for the determination of indentation locations. (d) The approximate position of the slice within the brain.

Horizontal mouse brain slices from 3 to 4 mm of dorsal-ventral positions of hippocampus (Fig. 7d) were submerged in a perfusion chamber assembled on the microscope, pressed down with a 2 mm spaced harp to assure stability, and supplied with a constant flow of carbogenated artificial cerebrospinal fluid (ACSF). Measurements were carried out on 9 slices from eight mice of which 6 were 6 months old and 2 – 9 months old. The indentation lines were selected to cross the DG and the subiculum or the CA3 field of hippocampus ($n \geq 66$ measurement points per slice). In addition, indentations on cortex were performed on 5 of the same slices adjacent to subiculum, in parallel lines between outer and inner layers ($n \geq 21$ measurement points per slice).

A ferrule-top force transducer [45], consisting of a micromachined cantilever spring with optical fiber readout, was mounted on a 3D printed holder screwed to a Z-piezoelectric actuator (PI p-603.5S2, Physik Instrumente). The single-mode fiber of the readout was coupled to an interferometer (OP1550, Optics11), where the interference signal was directly translated into cantilever deflection. Indentation depth control was implemented through a feedback loop, based on the error signal of cantilever deflection (Fig. 7, for more details see [46]). The piezoelectric actuator with the probe was mounted on a XYZ micromanipulator (PatchStar, Scientifica) for automatic mapping of mechanical properties. Indentation mapping was performed in parallel lines, with 59-476 points per slice. Distance between two adjacent locations

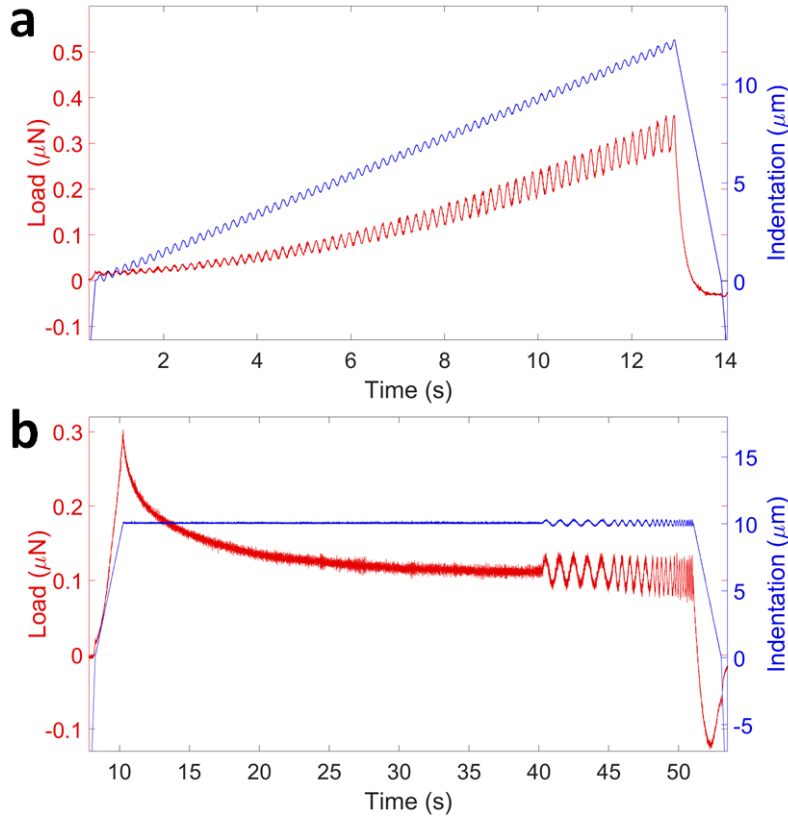


Figure 8: Depth-controlled indentation profiles. (a) Oscillatory ramp loading profile at 5.62 Hz oscillation frequency and (b) equilibrium frequency sweep profile between 1-10 Hz frequency range with both oscillation amplitudes of 0.2 μm .

were in the range of 50-160 μm , which assured that deformed areas do not overlap. A custom-written LabVIEW software (National Instruments) was used to process signals and to control the instrument through a data acquisition card (PCIe-6361, National Instruments).

Ferrule-top probes of 0.2-0.5 N/m stiffness and 60-105 μm bead radius were selected for these experiments and calibrated according to [68]. Two indentation-controlled profiles were selected for the characterization of depth and frequency dependent viscoelasticity: oscillatory ramp loading (OR) and equilibrium frequency sweep (FS). Fig. 8 shows the typical curves of the controlled-indentation and load response. Depth-controlled oscillatory ramp indentations (Fig. 8a) had small 0.2 μm oscillations at 5.62 Hz frequency superimposed on top of a loading ramp at 0.01 strain rate estimated by $\dot{\epsilon} \sim \Delta\epsilon/t$. Depth-controlled equilibrium frequency sweep measurements (Fig. 8b) consisted of the loading part up to 10 μm with 10 $\mu\text{m/s}$ indentation speed, followed by 30 s stress relaxation period to reach mechanical equilibrium and series of small ($h_0 = 0.2 \mu\text{m}$) sinusoidal oscillations at five distinct frequencies: 1, 1.78, 3.2, 5.62 and 10 Hz. The approach speed was set to 30 $\mu\text{m/s}$, the surface of the sample was determined, and an indentation-controlled feedback was triggered at approximate load of 15 nN, which resulted in the initial uncontrolled 1-3 μm indentation depth, which was later corrected in post processing procedures.

Data analysis

Raw data was analyzed with custom-written MATLAB functions. The Hertz model was used to fit an initial loading data up to the cantilever threshold value to obtain the true surface

position:

$$F = \frac{4}{3} \frac{E}{1 - \nu^2} \frac{R}{\sqrt{h^3}}, \quad (2)$$

where F is the load, E is an elastic modulus, ν is the Poisson's ratio of compressibility (we assume that brain is incompressible $\nu = 0.5$), h is the indentation depth. This allows us to correct the indentation depth h and estimate the strain for measurements with probes of different radius: $\varepsilon = 0.2 \times a/R$, where contact radius was estimated as $a = \sqrt{hR}$ varying between 22-39 μm . Strain of 7.3% was selected for comparative analysis in order to fulfill small strain approximation $\varepsilon < 0.08$ [69].

The sinusoidal oscillations were fit to cosine function, obtained amplitudes and phases were used to calculate the storage and loss moduli E' and E'' [46], which is a measure of elasticity and viscosity, respectively:

$$\frac{E'(\omega)}{1 - \nu^2} = \frac{F_0}{h_0} \cos\delta \frac{\sqrt{\pi}}{2} \frac{1}{\sqrt{A}}, \quad (3)$$

$$\frac{E''(\omega)}{1 - \nu^2} = \frac{F_0}{h_0} \sin\delta \frac{\sqrt{\pi}}{2} \frac{1}{\sqrt{A}} \quad (4)$$

where ω is the frequency, F_0 and h_0 are the amplitudes of oscillatory load and indentation depth, respectively, δ is the phase-shift between the recorded indentation and load oscillations, $A = \pi a^2$ is the contact area.

The contact area changes with the depth during oscillatory ramp, thus every 5 cycles were used for fitting and averaged indentation depth was used for the calculation of E' and E'' . Finally, all cosine fits with the $R^2 \leq 0.7$ and measurements which started in contact were rejected.

Normality of data distribution was tested with Shapiro-Wilk test ($n \geq 3$). In case of normal distribution, statistical differences between multiple groups were investigated with one-way ANOVA followed by Bonferroni *post hoc* test to achieve 95% confidence level ($\alpha = 0.05$). For non-normally distributed data, Kruskal-Wallis ANOVA test followed by Dunn's *post hoc* test with Šidák correction for $\alpha_1 = 1 - (1 - \alpha)^{1/k}$ was used to compare multiple groups. All statistical analyses were performed with Statistics and Machine Learning Toolbox (version 2017a, The Mathworks, Natick, MA, USA).

Code availability

The computer code used to generate the results of this study is available on request from the corresponding author.

Data availability

All raw and processed data that support the findings of this study are available from the corresponding author upon request.

Acknowledgements

The research leading to these results has received funding from the European Research Council under the European Union's Seventh Framework Programme (FP/20072013)/ERC grant

agreement no. [615170], the Dutch Technology Foundation (STW) under the iMIT program (P11-13) and Foundation for Fundamental Research on Matter (FOM), which is financially supported by the Netherlands Organisation for Scientific Research (NWO). The authors further thank M.Marrese, H.van Hoorn, T.Smit and L.Kooijman for fruitful discussions.

Author contributions

N.A., W.J.W., E.M.H. and D.I. designed the research; S.V.B. and N.A. performed the preliminary experiments; N.A. performed the experiments and analyzed the data; N.A. and D.I. wrote the manuscript; all authors contributed to the editing of the paper.

Competing interests

D.I. is co-founder and shareholder of Optics11.

References

- [1] Pouria Moshayedi, Gilbert Ng, Jessica C. F. Kwok, Giles S. H. Yeo, Clare E. Bryant, James W. Fawcett, Kristian Franze, and Jochen Guck. The relationship between glial cell mechanosensitivity and foreign body reactions in the central nervous system. *Biomaterials*, 35(13):3919–3925, April 2014.
- [2] Anna Jagielska, Adele L. Norman, Graeme Whyte, Krystyn J. Van Vliet, Jochen Guck, and Robin J. M. Franklin. Mechanical environment modulates biological properties of oligodendrocyte progenitor cells. *Stem Cells and Development*, 21(16):2905–2914, November 2012.
- [3] David E. Koser, Amelia J. Thompson, Sarah K. Foster, Asha Dwivedy, Eva K. Pillai, Graham K. Sheridan, Hanno Svoboda, Matheus Viana, Luciano da F. Costa, Jochen Guck, Christine E. Holt, and Kristian Franze. Mechanosensing is critical for axon growth in the developing brain. *Nature Neuroscience*, 19(12):1592–1598, December 2016.
- [4] Pouria Moshayedi, Luciano da F. Costa, Andreas Christ, Stephanie P. Lacour, James Fawcett, Jochen Guck, and Kristian Franze. Mechanosensitivity of astrocytes on optimized polyacrylamide gels analyzed by quantitative morphometry. *Journal of Physics. Condensed Matter: An Institute of Physics Journal*, 22(19):194114, May 2010.
- [5] D. Kacy Cullen, M. Christian Lessing, and Michelle C. LaPlaca. Collagen-dependent neurite outgrowth and response to dynamic deformation in three-dimensional neuronal cultures. *Annals of Biomedical Engineering*, 35(5):835–846, May 2007.
- [6] Penelope C. Georges, William J. Miller, David F. Meaney, Evelyn S. Sawyer, and Paul A. Janmey. Matrices with compliance comparable to that of brain tissue select neuronal over glial growth in mixed cortical cultures. *Biophysical Journal*, 90(8):3012–3018, April 2006.
- [7] Ana I. Teixeira, Shirin Ilkhanizadeh, Jens A. Wigenius, Joshua K. Duckworth, Olle Ingans, and Ola Hermanson. The promotion of neuronal maturation on soft substrates. *Biomaterials*, 30(27):4567–4572, September 2009.

- [8] Shantanu Sur, Christina J. Newcomb, Matthew J. Webber, and Samuel I. Stupp. Tuning supramolecular mechanics to guide neuron development. *Biomaterials*, 34(20):4749–4757, July 2013.
- [9] Lisa A. Flanagan, Yo-El Ju, Beatrice Marg, Miriam Osterfield, and Paul A. Janmey. Neurite branching on deformable substrates. *Neuroreport*, 13(18):2411–2415, December 2002.
- [10] Lars Bollmann, David E. Koser, Rajesh Shahapure, Hlne O. B. Gautier, Gerhard A. Holzapfel, Giuliano Scarcelli, Malte C. Gather, Elke Ulbricht, and Kristian Franze. Microglia mechanics: immune activation alters traction forces and durotaxis. *Frontiers in Cellular Neuroscience*, 9, September 2015.
- [11] La Chen, Wenfang Li, Vanessa Maybeck, Andreas Offenhusser, and Hans-Joachim Krause. Statistical study of biomechanics of living brain cells during growth and maturation on artificial substrates. *Biomaterials*, 106:240–249, November 2016.
- [12] Sanjay Kumar and Valerie M. Weaver. Mechanics, malignancy, and metastasis: the force journey of a tumor cell. *Cancer Metastasis Reviews*, 28(1-2):113–127, June 2009.
- [13] Claudia S. Barros, Santos J. Franco, and Ulrich Mller. Extracellular matrix: functions in the nervous system. *Cold Spring Harbor Perspectives in Biology*, 3(1):a005108, January 2011.
- [14] Marlene J. Vgh, Cline M. Heldring, Willem Kamphuis, Sara Hijazi, Arie J. Timmerman, Ka Wan Li, Pim van Nierop, Huibert D. Mansvelder, Elly M. Hol, August B. Smit, and Ronald E. van Kesteren. Reducing hippocampal extracellular matrix reverses early memory deficits in a mouse model of Alzheimer’s disease. *Acta Neuropathologica Communications*, 2:76, June 2014.
- [15] Haojie Mao, Benjamin S. Elkin, Vinay V. Genthikatti, Barclay Morrison, and King H. Yang. Why Is CA3 More Vulnerable Than CA1 in Experimental Models of Controlled Cortical Impact-Induced Brain Injury? *Journal of Neurotrauma*, 30(17):1521–1530, April 2013.
- [16] Antonio E. Forte, Stefano Galvan, Francesco Manieri, Ferdinando Rodriguez y Baena, and Daniele Dini. A composite hydrogel for brain tissue phantoms. *Materials & Design*, 112:227–238, December 2016.
- [17] Sean Jy-Shyang Chen, Pierre Hellier, Maud Marchal, Jean-Yves Gauvrit, Romain Carpentier, Xavier Morandi, and D. Louis Collins. An anthropomorphic polyvinyl alcohol brain phantom based on Colin27 for use in multimodal imaging. *Medical Physics*, 39(1):554–561, January 2012.
- [18] Kevin C. Spencer, Jay C. Sy, Khalil B. Ramadi, Ann M. Graybiel, Robert Langer, and Michael J. Cima. Characterization of Mechanically Matched Hydrogel Coatings to Improve the Biocompatibility of Neural Implants. *Scientific Reports*, 7(1):1952, May 2017.
- [19] Krishanu Saha, Albert J. Keung, Elizabeth F. Irwin, Yang Li, Lauren Little, David V. Schaffer, and Kevin E. Healy. Substrate Modulus Directs Neural Stem Cell Behavior. *Biophysical Journal*, 95(9):4426–4438, November 2008.
- [20] Albert J. Keung, Meimei Dong, David V. Schaffer, and Sanjay Kumar. Pan-neuronal maturation but not neuronal subtype differentiation of adult neural stem cells is mechanosensitive. *Scientific Reports*, 3:srep01817, May 2013.

- [21] Toms Luque, Michael S. Kang, David V. Schaffer, and Sanjay Kumar. Microelastic mapping of the rat dentate gyrus. *Royal Society Open Science*, 3(4), April 2016.
- [22] Till B. Puschmann, Carl Zandn, Yolanda De Pablo, Frank Kirchhoff, Marcela Pekna, Johan Liu, and Milos Pekny. Bioactive 3d cell culture system minimizes cellular stress and maintains the in vivo-like morphological complexity of astroglial cells. *Glia*, 61(3):432–440, March 2013.
- [23] Silvia Budday, Richard Nay, Rijk de Rooij, Paul Steinmann, Thomas Wyrobek, Timothy C. Ovaert, and Ellen Kuhl. Mechanical properties of gray and white matter brain tissue by indentation. *Journal of the Mechanical Behavior of Biomedical Materials*, 46:318–330, June 2015.
- [24] J. Weickenmeier, R. de Rooij, S. Budday, P. Steinmann, T. C. Ovaert, and E. Kuhl. Brain stiffness increases with myelin content. *Acta Biomaterialia*, 42:265–272, September 2016.
- [25] J. A. W. van Dommelen, T. P. J. van der Sande, M. Hrapko, and G. W. M. Peters. Mechanical properties of brain tissue by indentation: Interregional variation. *Journal of the Mechanical Behavior of Biomedical Materials*, 3(2):158–166, February 2010.
- [26] T. Kaster, I. Sack, and A. Samani. Measurement of the hyperelastic properties of ex vivo brain tissue slices. *Journal of Biomechanics*, 44(6):1158–1163, April 2011.
- [27] Yuan Feng, Ruth J. Okamoto, Ravi Namani, Guy M. Genin, and Philip V. Bayly. Measurements of mechanical anisotropy in brain tissue and implications for transversely isotropic material models of white matter. *Journal of the Mechanical Behavior of Biomedical Materials*, 23:117–132, July 2013.
- [28] Antonio E. Forte, Stephen M. Gentleman, and Daniele Dini. On the characterization of the heterogeneous mechanical response of human brain tissue. *Biomechanics and Modeling in Mechanobiology*, 16(3):907–920, June 2017.
- [29] Andreas F. Christ, Kristian Franze, Helene Gautier, Pouria Moshayedi, James Fawcett, Robin J. M. Franklin, Ragnhildur T. Karadottir, and Jochen Guck. Mechanical difference between white and gray matter in the rat cerebellum measured by scanning force microscopy. *Journal of Biomechanics*, 43(15):2986–2992, November 2010.
- [30] David E. Koser, Emad Moeendarbary, Janina Hanne, Stefanie Kuerten, and Kristian Franze. CNS Cell Distribution and Axon Orientation Determine Local Spinal Cord Mechanical Properties. *Biophysical Journal*, 108(9):2137–2147, May 2015.
- [31] Aref Samadi-Dooki, George Z. Voyiadjis, and Rhett W. Stout. An Indirect Indentation Method for Evaluating the Linear Viscoelastic Properties of the Brain Tissue. *Journal of Biomechanical Engineering*, 139(6), June 2017.
- [32] Isabell Weber, Seok-Hyun Yun, Guillano Scarcelli, and Kristian Franze. The role of cell body density in ruminant retina mechanics assessed by atomic force and Brillouin microscopy. *Physical Biology*, 2017.
- [33] John D. Finan, Erica M. Pearson, and Barclay Morrison. Viscoelastic properties of the rat brain in the horizontal plane. *Proceedings of the International Research Council on the Biomechanics of Injury conference*, 40:474–485, 2012.

- [34] Benjamin S. Elkin, Ashok Ilankova, and Barclay Morrison. Dynamic, regional mechanical properties of the porcine brain: indentation in the coronal plane. *Journal of Biomechanical Engineering*, 133(7):071009, July 2011.
- [35] Benjamin S. Elkin and Barclay Morrison. Viscoelastic properties of the P17 and adult rat brain from indentation in the coronal plane. *Journal of Biomechanical Engineering*, 135(11):114507, November 2013.
- [36] Benjamin S. Elkin, Ashok Ilankovan, and Barclay Morrison. Age-dependent regional mechanical properties of the rat hippocampus and cortex. *Journal of Biomechanical Engineering*, 132(1):011010, January 2010.
- [37] John D. Finan, Benjamin S. Elkin, Erica M. Pearson, Irene L. Kalbian, and Barclay Morrison. Viscoelastic Properties of the Rat Brain in the Sagittal Plane: Effects of Anatomical Structure and Age. *Annals of Biomedical Engineering*, 40(1):70–78, January 2012.
- [38] G. Franceschini, D. Bigoni, P. Regitnig, and G. A. Holzapfel. Brain tissue deforms similarly to filled elastomers and follows consolidation theory. *Journal of Mechanics Physics of Solids*, 54:2592–2620, December 2006.
- [39] M. Hrapko, J. a. W. van Dommelen, G. W. M. Peters, and J. S. H. M. Wismans. The influence of test conditions on characterization of the mechanical properties of brain tissue. *Journal of Biomechanical Engineering*, 130(3):031003, June 2008.
- [40] S. Budday, G. Sommer, C. Birkl, C. Langkammer, J. Haybaeck, J. Kohnert, M. Bauer, F. Paulsen, P. Steinmann, E. Kuhl, and G. A. Holzapfel. Mechanical characterization of human brain tissue. *Acta Biomaterialia*, 48:319–340, January 2017.
- [41] Kevin M. Labus and Christian M. Puttlitz. An anisotropic hyperelastic constitutive model of brain white matter in biaxial tension and structural-mechanical relationships. *Journal of the Mechanical Behavior of Biomedical Materials*, 62:195–208, September 2016.
- [42] Simon Chatelin, Andr Constantinesco, and Rmy Willinger. Fifty years of brain tissue mechanical testing: From in vitro to in vivo investigations. *Biorheology*, 47(5-6):255–276, January 2010.
- [43] Benjamin S. Elkin, Evren U. Azeloglu, Kevin D. Costa, and Barclay Morrison. Mechanical heterogeneity of the rat hippocampus measured by atomic force microscope indentation. *Journal of Neurotrauma*, 24(5):812–822, May 2007.
- [44] Shaokoon Cheng, Elizabeth C. Clarke, and Lynne E. Bilston. Rheological properties of the tissues of the central nervous system: a review. *Medical Engineering & Physics*, 30(10):1318–1337, December 2008.
- [45] D. Chavan, T. C. van de Watering, G. Gruca, J. H. Rector, K. Heeck, M. Slaman, and D. Iannuzzi. Ferrule-top nanoindenter: An optomechanical fiber sensor for nanoindentation. *Review of Scientific Instruments*, 83(11):115110, November 2012.
- [46] Hedde van Hoorn, Nicholas A. Kurniawan, Gijsje H. Koenderink, and Davide Iannuzzi. Local dynamic mechanical analysis for heterogeneous soft matter using ferrule-top indentation. *Soft Matter*, 12(12):3066–3073, 2016.
- [47] Steven V. Beekmans, Kaj S. Emanuel, Theodoor H. Smit, and Davide Iannuzzi. Minimally Invasive Micro-Indentation: mapping tissue mechanics at the tip of an 18g needle. *Scientific Reports*, 7, September 2017.

- [48] S. V. Beekmans and D. Iannuzzi. Characterizing tissue stiffness at the tip of a rigid needle using an opto-mechanical force sensor. *Biomedical Microdevices*, 18(1):15, February 2016.
- [49] John D. Finan, Sowmya N. Sundaresh, Benjamin S. Elkin, Guy M. McKhann, and Barclay Morrison. Regional mechanical properties of human brain tissue for computational models of traumatic brain injury. *Acta Biomaterialia*, 55(Supplement C):333–339, June 2017.
- [50] D. W. Brands, P. H. Bovendeerd, G. W. Peters, and J. S. Wismans. The large shear strain dynamic behaviour of in-vitro porcine brain tissue and a silicone gel model material. *Stapp Car Crash Journal*, 44:249–260, November 2000.
- [51] M. Hrapko, J. a. W. van Dommelen, G. W. M. Peters, and J. S. H. M. Wismans. The mechanical behaviour of brain tissue: Large strain response and constitutive modelling. *Biorheology*, 43(5):623–636, January 2006.
- [52] G. W. M. Peters, J. H. Meulman, and A. A. H. J. Sauren. The applicability of the time/temperature superposition principle to brain tissue. *Biorheology*, 34(2):127–138, March 1997.
- [53] F. Shen, T. E. Tay, J. Z. Li, S. Nigen, P. V. S. Lee, and H. K. Chan. Modified Bilston non-linear viscoelastic model for finite element head injury studies. *Journal of Biomechanical Engineering*, 128(5):797–801, October 2006.
- [54] S. Chatelin, J. Vappou, S. Roth, J. S. Raul, and R. Willinger. Towards child versus adult brain mechanical properties. *Journal of the Mechanical Behavior of Biomedical Materials*, 6:166–173, February 2012.
- [55] A. Garo, M. Hrapko, J. a. W. van Dommelen, and G. W. M. Peters. Towards a reliable characterisation of the mechanical behaviour of brain tissue: The effects of post-mortem time and sample preparation. *Biorheology*, 44(1):51–58, 2007.
- [56] Jonathan Vappou, Elodie Breton, Philippe Choquet, Christian Goetz, Rmy Willinger, and Andr Constantinesco. Magnetic resonance elastography compared with rotational rheometry for in vitro brain tissue viscoelasticity measurement. *Magnetic Resonance Materials in Physics, Biology and Medicine*, 20(5-6):273, December 2007.
- [57] Michael T. Prange and Susan S. Margulies. Regional, Directional, and Age-Dependent Properties of the Brain Undergoing Large Deformation. *Journal of Biomechanical Engineering*, 124(2):244–252, March 2002.
- [58] Thomas Grevesse, Bornha E. Dabiri, Kevin Kit Parker, and Sylvain Gabriele. Opposite rheological properties of neuronal microcompartments predict axonal vulnerability in brain injury. *Scientific Reports*, 5:srep09475, March 2015.
- [59] Dafna Bonne-Barkay and Clayton A. Wiley. Brain Extracellular Matrix in Neurodegeneration. *Brain Pathology*, 19(4):573–585, October 2009.
- [60] David C. Van Essen. A tension-based theory of morphogenesis and compact wiring in the central nervous system. *Nature*, 385(6614):313–318, January 1997.
- [61] Henry W. Haslach, Lauren N. Leahy, Peter Riley, Rao Gullapalli, Su Xu, and Adam H. Hsieh. Solidextracellular fluid interaction and damage in the mechanical response of rat brain tissue under confined compression. *Journal of the Mechanical Behavior of Biomedical Materials*, 29:138–150, January 2014.

- [62] Kristian Franze. The mechanical control of nervous system development. *Development (Cambridge, England)*, 140(15):3069–3077, August 2013.
- [63] Kristian Franze and Jochen Guck. The biophysics of neuronal growth. *Reports on Progress in Physics*, 73:094601, September 2010.
- [64] Gang Xu, Philip V. Bayly, and Larry A. Taber. Residual stress in the adult mouse brain. *Biomechanics and modeling in mechanobiology*, 8(4):253–262, August 2009.
- [65] Gang Xu, Andrew K. Knutsen, Krikor Dikranian, Christopher D. Kroenke, Philip V. Bayly, and Larry A. Taber. Axons Pull on the Brain, But Tension Does Not Drive Cortical Folding. *Journal of Biomechanical Engineering*, 132(7):071013–071013–8, June 2010.
- [66] Claus C. Hilgetag and Helen Barbas. Role of Mechanical Factors in the Morphology of the Primate Cerebral Cortex. *PLOS Computational Biology*, 2(3):e22, 2006.
- [67] Shawn Mikula, Issac Trotts, James M. Stone, and Edward G. Jones. Internet-Enabled High-Resolution Brain Mapping and Virtual Microscopy. *NeuroImage*, 35(1):9–15, March 2007.
- [68] S. V. Beekmans and D. Iannuzzi. A metrological approach for the calibration of force transducers with interferometric readout. *Surface Topography: Metrology and Properties*, 3(2):025004, 2015.
- [69] David C. Lin, David I. Shreiber, Emiliós K. Dimitriadis, and Ferenc Horkay. Spherical indentation of soft matter beyond the Hertzian regime: numerical and experimental validation of hyperelastic models. *Biomechanics and modeling in mechanobiology*, 8(5):345–358, October 2009.